Geochimica et Cosmochimica Acta, Vol. 69, No. 4, pp. 825–837, 2005

0016-7037/05 $30.00 + .00

doi:10.1016/j.gca.2004.06.012

Theoretical investigation of iron isotope fractionation between $Fe(H_2O)_6^{3+}$ and $Fe(H_2O)_6^{2+}$: Implications for iron stable isotope geochemistry

A. D. Anbar,[1,2,*†] A. A. Jarzecki,[3,4] and T. G. Spiro[3,4]

[1]Department of Earth and Environmental Sciences, University of Rochester, Rochester, New York 14627 USA
[2]Department of Chemistry, University of Rochester, Rochester, New York 14627 USA
[3]Department of Chemistry, Princeton University, Princeton, New Jersey 08544 USA
[4]Center for Environmental Bioinorganic Chemistry, Princeton University, Princeton, New Jersey 08544 USA

(*Received August* 15, 2003; *accepted in revised form June* 14, 2004)

Abstract—The magnitude of equilibrium iron isotope fractionation between $Fe(H_2O)_6^{3+}$ and $Fe(H_2O)_6^{2+}$ is calculated using density functional theory (DFT) and compared to prior theoretical and experimental results. DFT is a quantum chemical approach that permits a priori estimation of all vibrational modes and frequencies of these complexes and the effects of isotopic substitution. This information is used to calculate reduced partition function ratios of the complexes ($10^3 \cdot \ln(\beta)$), and hence, the equilibrium isotope fractionation factor ($10^3 \cdot \ln(\alpha)$). Solvent effects are considered using the polarization continuum model (PCM). DFT calculations predict fractionations of several per mil in $^{56}Fe/^{54}Fe$ favoring partitioning of heavy isotopes in the ferric complex. Quantitatively, $10^3 \cdot \ln(\alpha)$ predicted at 22°C, ~ 3 ‰, agrees with experimental determinations but is roughly half the size predicted by prior theoretical results using the Modified Urey-Bradley Force Field (MUBFF) model. Similar comparisons are seen at other temperatures. MUBFF makes a number of simplifying assumptions about molecular geometry and requires as input IR spectroscopic data. The difference between DFT and MUBFF results is primarily due to the difference between the DFT-predicted frequency for the ν_4 mode (O-Fe-O deformation) of $Fe(H_2O)_6^{3+}$ and spectroscopic determinations of this frequency used as input for MUBFF models (185–190 cm^{-1} vs. 304 cm^{-1}, respectively). Hence, DFT-PCM estimates of $10^3 \cdot \ln(\beta)$ for this complex are ~ 20% smaller than MUBFF estimates. The DFT derived values can be used to refine predictions of equilibrium fractionation between ferric minerals and dissolved ferric iron, important for the interpretation of Fe isotope variations in ancient sediments. Our findings increase confidence in experimental determinations of the $Fe(H_2O)_6^{3+} - Fe(H_2O)_6^{2+}$ fractionation factor and demonstrate the utility of DFT for applications in "heavy" stable isotope geochemistry. *Copyright © 2005 Elsevier Ltd*

1. INTRODUCTION

The stable isotope geochemistry of "heavy" elements, especially transition metals, has emerged as a vibrant area in geochemical research. Mass-dependent variations in the isotopic compositions of Cu, Zn, Fe, Cr, Mo, Cd, and even Tl have been reported in nature (e.g., Beard and Johnson, 1999; Beard et al., 1999; Marechal et al., 1999; Zhu et al., 2000; Barling et al., 2001; Brantley et al., 2001; Bullen et al., 2001; Sharma et al., 2001; Ellis et al., 2002; McManus et al., 2002; Rehkamper et al., 2002; Walczyk and von Blanckenburg, 2002; Beard et al., 2003; Johnson et al., 2003a; Siebert et al., 2003; Wombacher et al., 2003; Arnold et al., 2004a). Fe isotope research has drawn particular attention because of the ubiquity of this element in the environment and its importance in biology. As a result, Fe isotope geochemistry may prove useful in a range of biogeoscience applications (e.g., Anbar, 2004). For example, Fe isotope variations in Precambrian Banded Iron Formations (BIF) have been interpreted as providing evidence of biologically mediated Fe redox cycling (Beard et al., 1999; Johnson et al., 2003a).

Transition metal isotope research has been driven almost exclusively by advances in analytical capabilities, especially developments in multiple-collector inductively coupled plasma mass spectrometry (MC-ICP-MS) (Halliday et al., 1995; Marechal et al., 1999; Belshaw et al., 2000; Johnson et al., 2002; Arnold et al., 2004b). In contrast, there has been little investigation of transition metal isotope fractionation from a theoretical standpoint. Reliable theoretical models would increase confidence in experimental determinations of metal isotope fractionation factors. Such models would also make it possible to estimate the magnitude of isotope fractionation resulting from reactions that are not experimentally tractable. Without such estimates, it will be difficult to determine the causes of isotope fractionation in complex natural systems.

In the case of Fe isotopes, equilibrium fractionation between dissolved $Fe(H_2O)_6^{2+}$ and $Fe(H_2O)_6^{3+}$ is particularly important because of the large difference in energies between ferric and ferrous bonds to the same ligands and because these are major Fe species in solution (especially at acidic pH). However, experimental and theoretical investigations of the magnitude of equilibrium isotope fractionation between these species have not converged.

In the first examinations of redox-associated Fe isotope fractionation, effects of ~1‰ in $^{56}Fe/^{54}Fe$ were seen during microbially mediated reduction of ferrihydrite (Beard et al., 1999), and during oxidation of dissolved Fe(II) to form ferrihydrite in natural and laboratory systems (Bullen et al., 2001). In all cases, $^{56}Fe/^{54}Fe$ was larger in ferric phases. However, these

* Author to whom correspondence should be addressed (anbar@asu.edu).
† *Present address:* Department of Geological Sciences and Department of Chemistry & Biochemistry, Arizona State University, Tempe, Arizona 85287-1404 USA.

experiments were not designed for rigorous determination of equilibrium isotope effects. Such determinations are not trivial because it is necessary to separate the complexes after attainment of isotopic equilibrium without perturbing this equilibrium (or with careful calibration of the extent of perturbation). Initial experimental efforts were complicated by large kinetic isotope effects (Matthews et al., 2001). In the first study attempting to address this problem, Johnson et al. (2002) reported an experimentally determined $^{56}Fe/^{54}Fe$ equilibrium fractionation of $\sim 2.75 \pm 0.30$ ‰ ($\pm 2\sigma$) between $Fe(H_2O)_6^{2+}$ and $Fe(H_2O)_6^{3+}$ at 22°C. The value of the fractionation factor was subsequently refined to $\sim 3.00 \pm 0.46$ ‰ ($\pm 2\sigma$) (Welch et al., 2003). These are the most refined such studies.

Theoretical examination of dissolved ferric-ferrous isotope fractionation is confined to the pioneering work of Schauble et al. (2001), who used published vibrational spectroscopic data for a number of Fe complexes and an empirical force field model (the "Modified Urey-Bradley Force Field"; MUBFF) to estimate shifts in vibrational frequencies upon isotope substitution. These estimates were used to predict equilibrium isotope fractionation. For $Fe(H_2O)_6^{2+}$ and $Fe(H_2O)_6^{3+}$, $^{56}Fe/^{54}Fe$ fractionation of ~5.4‰ was predicted at 25°C. This is the only theoretical estimate of the fractionation between $Fe(H_2O)_6^{2+}$ and $Fe(H_2O)_6^{3+}$ published to date.

The difference between the experimental and theoretical findings translates to about a twofold difference in the expected variation of the ratio $^{56}Fe/^{54}Fe$ between ferric and ferrous hexa-aquo complexes. It has been suggested that this difference indicates a deficiency in the theoretical results (Johnson et al., 2002; Skulan et al., 2002). However, there is some dispute as to whether isotopic equilibrium was attained in all experiments, particularly at near-neutral pH (Bullen et al., 2003; Johnson et al., 2003b). As a result, there is considerable uncertainty surrounding the equilibrium fractionation factors between dissolved ferrous and ferric complexes. Clearly, such uncertainty must be resolved.

Density functional theory (DFT), a more sophisticated approach than MUBFF, has not yet been used to estimate transition metal isotope fractionation effects. Here, we report the results of a DFT investigation of isotope-sensitive vibrational modes and frequencies of $Fe(H_2O)_6^{2+}$ and $Fe(H_2O)_6^{3+}$ isotopomers (a more complete DFT investigation of vibrational modes can be found in a companion paper, Jarzecki et al. (2004)). Theoretical equilibrium isotope fractionation factors between these complexes generated from the DFT results are compared to prior theoretical and experimental results. Implications for Fe stable isotope geochemistry are discussed.

2. THEORY AND METHODS

2.1. Isotope Fractionation

In principle, theoretical modeling of equilibrium isotope effects is straightforward if vibrational frequencies of isotopically substituted compounds are known. Complications arise from the need to obtain these vibrational frequencies from infrared (IR) spectroscopy or theory.

The general approach was developed by Urey, and Bigeleisen and Mayer (Bigeleisen and Mayer, 1947; Urey, 1947), and has been reviewed repeatedly (e.g., O'Neil, 1986; Criss, 1999; Schauble et al., 2004). It is summarized here briefly to define notation, to clarify the essential practical differences between use of DFT and MUBFF methods to obtain vibrational frequencies, and to orient nonspecialist readers to the key issues.

Equilibrium isotope fractionation between $Fe(H_2O)_6^{2+}$ and $Fe(H_2O)_6^{3+}$ can be considered in terms of an equilibrium isotope exchange reaction:

$$^{56}Fe(H_2O)_6^{2+} + {}^{54}Fe(H_2O)_6^{3+} \rightleftarrows {}^{56}Fe(H_2O)_6^{3+} + {}^{54}Fe(H_2O)_6^{2+} \quad (1)$$

Equilibrium isotope fractionation stems primarily from the differences in molecular vibrational energies between the isotopomers of the ferric and ferrous complexes (vibrational modes involving motion of the central Fe atom being sensitive to isotope substitution). As a result of these differences, the equilibrium constant for this reaction, $K, \neq 1$. By definition, the equilibrium fractionation factor for this exchange reaction, α, is equivalent to K; a slightly more complex relationship is obtained in reactions involving exchange of more than one atom. α can be obtained from the "reduced" partition function ratios, β_{56-54}:

$$\alpha = \beta_{56-54}(Fe(H_2O)_6^{3+})/\beta_{56-54}(Fe(H_2O)_6^{2+}) \quad (2)$$

The reduced partition function ratio of each complex is given by

$$\beta_{56-54} = \prod_{i=1}^{3N-6} \frac{^{56}U_i}{^{54}U_i} \cdot \frac{^{56}Q_{vib}}{^{54}Q_{vib}} = \prod_{i=1}^{3N-6} \frac{^{56}U_i}{^{54}U_i} \cdot \frac{e^{-^{56}U_i/2}}{e^{-^{54}U_i/2}} \cdot \frac{1 - e^{-^{54}U_i}}{1 - e^{-^{56}U_i}} \quad (3)$$

where

$$U_i = \frac{h\nu_i}{k\mathrm{T}} \quad (4)$$

Here, h and k are the Planck and Boltzmann constants, respectively, T is temperature, N is the number of atoms in the complex (hence, $3N$-6 is the number of vibrations), Q_{vib} are vibrational partition functions, and ν_i are the vibrational frequencies for the two isotopomers of each complex. Symmetry factors are omitted because they have no effect on isotope fractionation.

It follows straightforwardly that the isotope fractionation at equilibrium between $Fe(H_2O)_6^{2+}$ and $Fe(H_2O)_6^{3+}$ can be predicted if ν_i of the isotopomers are known. For effects of the magnitude seen in the Fe isotope system, the magnitude of this fractionation is $\sim 10^3 \cdot \ln(\alpha)$.

An alternative approach uses ^{57}Fe Mössbauer spectroscopic data to predict equilibrium isotope fractionation factors between Fe-bearing minerals and other substances for which such data are available (Polyakov, 1997; Polyakov and Mineev, 2000). However, because the Mössbauer effect is confined to solids, the utility of this method for aqueous species is limited. It is also not extensible to many transition metals other than Fe.

2.2. Molecular Vibrations and Force Field Models

In practice, experimentally determined vibrational spectra for isotopically substituted complexes are seldom available. This is the case for $Fe(H_2O)_6^{2+}$ and $Fe(H_2O)_6^{3+}$. Therefore, to calculate β_{56-54}, at least some frequencies must be obtained theoretically.

If the spectrum of at least one isotopomer of each species is available, it is possible to predict the isotopic shift in vibrational frequencies using a suitable molecular force-field model and to use these predictions as the basis for an isotope fractionation prediction. This was the approach taken by Schauble et al. (2001), utilizing experimental vibrational data drawn from the literature for isotopically "normal" complexes. Because the natural isotopic abundance of ^{56}Fe is ~91.2%, these experimental data are a good approximation for the ^{56}Fe isotopomers. Schauble et al. (2001) used the MUBFF model, widely used for gases of light isotopes (e.g., Richet et al., 1977).

In many cases of geochemical relevance, vibrational data are entirely unavailable. Additionally, even when experimental vibrational data are available in the literature, the assignment of particular IR absorption features to particular vibrational modes is sometimes questionable. For both these reasons, it is desirable to use a force-field model that is capable of accurate a priori prediction of vibrational frequencies, eliminating the need for experimental data as input. This is not possible with MUBFF.

MUBFF is also limited in assuming idealized molecular symmetry, e.g., nominally octahedral complexes like Fe-aquo complexes are assumed to be perfect octahedra. This idealization substantially simplifies the calculation of vibrational effects arising from isotopic substitution

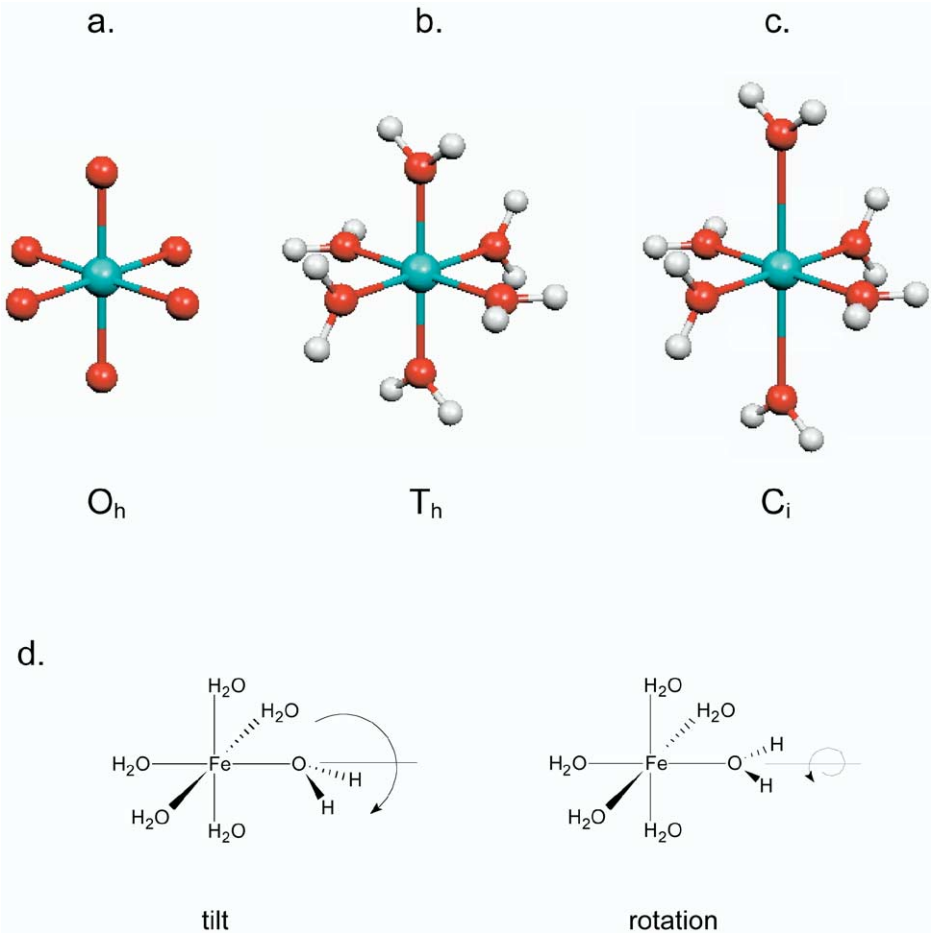

Fig. 1. Illustration of (a) the skeletal FeO_6 octahedron (O_h symmetry); (b) the water orientations in the T_h structure of $Fe(H_2O)_6^{3+}$; (c) the Jahn-Teller distorted C_i structure of $Fe(H_2O)_6^{2+}$ (distortion exaggerated for clarity); and (d) the H_2O tilting and rotation coordinates that lower $Fe(H_2O)_6^{3+}$ symmetry from T_h to S_6 (distortions permitted in the C_i symmetry group).

of the central atom. However, a consequence of this idealization is that geometric distortions, such as those arising from the Jahn-Teller effect, are ignored. Symmetry is further reduced by the presence of molecular ligands like H_2O, and by rotation and/or tilting of these ligands (Fig. 1). Additionally, there may be vibrational modes of the complex in which motions of the central atom couple to vibrations of bonds in the ligands (Fig. 2). These factors, potentially important when modeling aquo complexes, are ignored by MUBFF. For this reason, a theoretical method more sophisticated than MUBFF is desired, even when reliable spectral data are available for one isotopomer of each complex.

In principle, various ab initio models could be applied, solving the complete Schrödinger equations and finding a wave function for each complex. However, attaining accurate results with such methods is generally not as computationally efficient as with density functional theory (DFT). DFT methods provide a better tradeoff between accuracy and efficiency. For this reason, the use of DFT to approach problems of a chemical nature has increased dramatically in recent years. Modern DFT has its fundamental roots in the theorems of Hohenberg and Kohn (1964), which demonstrate that the energy of a many-electron system can be expressed in terms of its electron density. This greatly simplifies

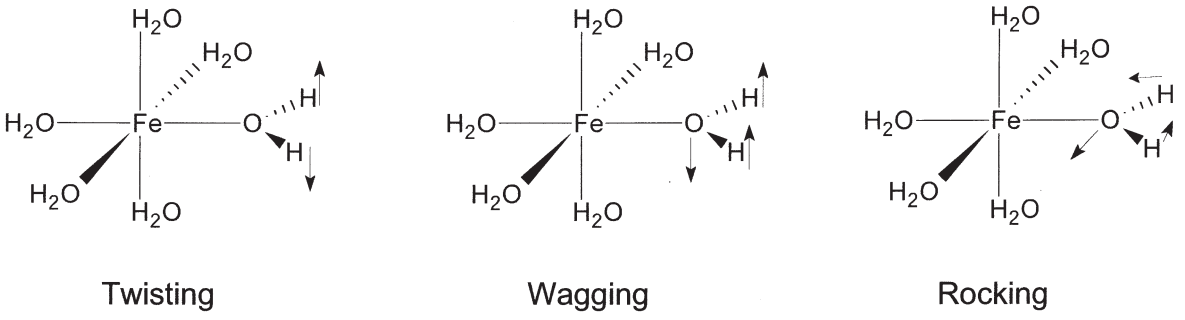

Fig. 2. Schematic representation of twisting, wagging, and rocking vibrational coordinates of bound H_2O.

Table 1. Calculated and experimental bond distances (Å) and angles (°) in $Fe(H_2O)_6^{3+}$.

	DFT[a]	DFT-PCM[b]		$CsFe(SO_4)_2 \cdot 12H_2O$[c]	$CsFe(SeO_4)_2 \cdot 12H_2O$[c]
Symmetry:	T_h	T_h[d]	S_6[e]	S_6	S_6
Fe-O	2.039	1.996	2.005	1.994 (1)	2.002 (1)
O-Fe-O	90.00	90.00	90.01	90.9 (1)	90.5 (1)
O-H	0.982	0.995	0.998	0.995 (3)	1.002 (2)
H-O-H	106.76	108.28	107.31	110.4 (2)	108.0 (2)
Fe-OH_2 tilt	0.00	0.00	24.83	0.6 (10)	18.6 (10)
Fe-OH_2 rot.	0.00	0.00	4.77		

[a] B3LYP/6-31G* and Ahlrichs' VTZ level of theory (*in vacuo.*)
[b] PCM B3LYP/6-31G* & Ahlrichs' VTZ level of theory in polarizable continuum model ($\varepsilon = 78.4$).
[c] Low-temperature neutron diffraction data (Best and Forsyth, 1990).
[d] Constrained to T_h symmetry.
[e] Fully optimized PCM structure.

the wave function of a system, but recent forms of density functionals have been shown to produce highly accurate results. Detailed reviews of DFT can be found elsewhere (e.g., Laird et al., 1996).

Within the DFT approach, it is also possible to compute solvent effects. For example, the polarizable continuum model (PCM), is one of the most used and reliable continuum solvation procedures (Miertus et al., 1981; Cammi and Tomasi, 1995; Cossi et al., 1996; Cances et al., 1997; Mennucci et al., 1997; Amovilli et al., 1999; Cammi and Mennucci, 1999; Mennucci et al., 1999; Cossi and Barone, 2001; Cossi et al., 2001). Using the PCM, the solute is placed in a polarizable cavity formed by an envelope of spheres centered on the atoms or the atomic groups. Inside the cavity the dielectric constant is the same as in vacuo, while outside it takes the value of the desired solvent [$\varepsilon = 78.4$ for pure water]. This approach accounts for the effect of nondirectional (i.e., excluding H-bonding) polarization effects of solvent H_2O molecules on vibrations of the complexes. In this study we report results from DFT calculations of the complexes both in hypothetical gas phase (in vacuo) and in simulated solvent (DFT-PCM).

As shown below, PCM modeling correctly predicts that Fe-O stretch frequencies shift up when complexes are solvated, and in fact, better matches vibrational data (Table 3). This improvement is consistent with an approach taken by Rudolph and Pye (2000), in which a solvation layer was built by adding explicit water molecules. Although the PCM approach is a computationally efficient and commonly applied method to model solvation effects on molecular structure and frequencies, explicit tests on aquo complexes have not been performed. Our computations indicate that DFT-PCM models predict expected shifts in frequencies, but prediction of structures might require more elaborate methods to build the polarizable cavity for aquo complexes.

2.3. Computational Methods

Computations were performed with the Gaussian 98 program package (Frisch et al., 1998), using the B3LYP gradient-corrected hybrid density functional to optimize structures and calculate vibrational frequencies. This functional combines Becke's three-parameter hybrid of the gradient-corrected exchange (B3) (Becke, 1993a; Becke, 1993b) and the exact HF (Hartree-Fock) exchange with the Lee, Yang, and Parr (LYP) gradient-corrected correlation functional (Lee et al., 1988).

For the basis set functions, we applied the 5-d component set, comprised of the standard 6 to 31G* basis functions on the O and H atoms (Ditchfield et al., 1971; Hehre et al., 1972; Hariharan and Pople, 1973; Hariharan and Pople, 1974; Francl et al., 1982; Rassolov et al., 1998), and Ahlrichs' valence triple-ζ (VTZ) basis set on the Fe atom (Schafer et al., 1992). Previous applications of the B3LYP functional in combination with these basis sets produced quite reliable structures and frequencies for various transition metal complexes (Diaz-Acosta et al., 2001; Diaz-Acosta et al., 2003) and metalloporphyrins (Jarzecki et al., 1997; Kozlowski et al., 1999).

Since the aquo ions are well-known to be high-spin, only the sextet state for Fe^{3+} and the quintet state for Fe^{2+} were evaluated. The complexes were treated in vacuo and then embedded in the PCM to account for the presence of solvent.

There is no systematic way to define the uncertainties on vibrational frequencies predicted by this method. However, prior experience with transition metal-ligand bonds indicates that predicted frequencies are generally within $\pm$ 25 cm^{-1} of experimental values (Diaz-Acosta et al., 2001). We adopt this as a conservative estimate of the 95% confidence interval for DFT predictions.

Predicted vibrational frequencies for the isotopomers of both compounds were then used to obtain β_{56-54} following Eqn. 3. In practice we calculated $\ln(\beta_{56-54})$ by subtracting from $\ln({}^{56}Q_{vib}/{}^{54}Q_{vib})$ a constant, $\ln[({}^{56}m/{}^{54}m)^{3/2} \cdot ({}^{54}M/{}^{56}M)^{3/2}]$, where ${}^{n}m$ are the isotope masses and ${}^{n}M$ are the masses of the isotopomers. This constant is equivalent to $\prod_{i=1}^{3N-6} \frac{{}^{56}U_i}{{}^{54}U_i}$ via the Redlich-Teller product rule (Wilson et al., 1955). For ^{56}Fe, ^{54}Fe and the hexa-aquo complexes, and using integer masses, the value of this constant is 3.6124×10^{-2}.

In experimental studies, isotope fractionation is generally reported as the parts-per-thousand (‰) deviation in the ratio $^{56}Fe/^{54}Fe$ between the two complexes, Δ, where $\Delta \sim 10^3 \cdot \ln(\alpha) = 10^3 \cdot \ln(\beta_{56-54}(Fe(H_2O)_6^{3+})) - 10^3 \cdot \ln(\beta_{56-54}(Fe(H_2O)_6^{2+}))$. Hence, it has become conventional in theoretical studies to tabulate reduced partition function ratios in terms of $10^3 \cdot \ln(\beta_{56-54})$ (Polyakov, 1997; Polyakov and Mineev, 2000; Schauble et al., 2001). We follow this convention here.

3. RESULTS AND DISCUSSION

3.1. Structures

Comparison of theoretical bond lengths and angles with experimental data provides a means of testing DFT models. There are no experimental data on structures of these complexes in vacuo or solution, but crystallographic data are available for ferric and ferrous salts. Computed structural parameters for $Fe(H_2O)_6^{2+}$ and $Fe(H_2O)_6^{3+}$ are given in Tables 1 and 2, along with relevant experimental data.

We are especially interested in comparisons of bond lengths because of the correlation with bond strengths, and hence, vibrational frequencies; if the models do not reasonably reproduce experimental bond lengths, then predicted vibrational frequencies are suspect. As discussed below, the agreement between model results and experiments is good.

3.1.1. $Fe(H_2O)_6^{3+}$

The $Fe(H_2O)_6^{3+}$ complex was initially optimized as a FeO_6 octahedron with the water H atoms arranged in T_h symmetry (Fig. 1). This procedure converged to a structure with all

Table 2. Calculated and experimental bond distances (Å) and angles (°) in $Fe(H_2O)_6^{2+}$.

	DFT[a] C_i	DFT-PCM[b] C_i	Ammonium Tutton Salt[c] $(NH_4)_2[Fe(H_2O)_6]SO_4$
Fe-O_1	2.140	2.125	2.143 (2)
Fe-O_2	2.136	2.106	2.136 (2)
Fe-O_3	2.110	2.086	2.098 (2)
O_1-Fe-O_2	89.99	89.66	89.25 (6)
O_1-Fe-O_3	91.19	91.33	91.02 (6)
O_2-Fe-O_3	90.01	90.10	90.86 (6)
H-O_1	0.973	0.982	0.83 (3)
H-O_2	0.973	0.983	0.82 (3)
H-O_3	0.973	0.980	0.95 (3)
H-O_1-H	106.45	105.07	-
H-O_2-H	106.74	105.72	-
H-O_3-H	106.85	106.50	-
Fe-O_1H_2 tilt	0.06	34.48	-
Fe-O_1H_2 rot	9.38	28.19	-
Fe-O_2H_2 tilt	0.62	39.62	-
Fe-O_2H_2 rot	4.82	10.59	-
Fe-O_3H_2 tilt	4.02	9.13	-
Fe-O_3H_2 rot	0.14	7.30	-

[a] B3LYP/6-31G* & Ahlrichs' VTZ level of theory (*in vacuo*).
[b] PCM B3LYP/6-31G* and Ahlrichs' VTZ level of theory in polarizable continuum model (ε = 78.4).
[c] X-ray data (Cotton et al., 1993). Dashes indicate experimental data not reported.

positive vibrational frequencies in vacuo. However, in the PCM model three frequencies were negative, suggesting that this was not the lowest energy configuration. Removal of the T_h symmetry constraint, allowing realignment of the water molecules, led to a S_6 PCM structure in which the water molecules are tilted and rotated with respect to the FeO_4 planes (Fig. 1). The energy was lowered by 1.7 kcal/mol. In Table 1, bond lengths and angles for all three structures (T_h in vacuo, and T_h and S_6 PCM) are compared to low-temperature neutron data for Fe cesium sulphate and selenate alums, $CsFe(SO_4)_2 \cdot 12H_2O$ and $CsFe(SeO_4)_2 \cdot 12H_2O$ (structurally, these are β and α alums, respectively) (Best and Forsyth, 1990).

The predicted Fe-O bond lengths in $Fe(H_2O)_6^{3+}$ are all equal, because Fe^{3+} has a d^5 electron configuration and is spherically symmetric. The predicted Fe-O distance in $Fe(H_2O)_6^{3+}$ is 2.039 Å in vacuo but decreases by ~ 0.04 Å in the PCM model, bringing it into good agreement with the alum structures (1.994 and 2.002 Å). Thus PCM appears to improve the main structure parameter in the case of $Fe(H_2O)_6^{3+}$.

The computed O-H distances for $Fe(H_2O)_6^{3+}$ are 0.982 Å in vacuo, and increase to 0.995 Å (T_h structure) or 0.998 Å (S_6 structure) in the PCM model, in better agreement with the neutron structures of the alums.

However, upon closer examination, the tilt and rotation of the water molecules in the S_6 structure were found to be artifacts of the PCM methodology, which imposes a spherical cavity of fixed dimension. Energy comparisons with an adjustable cavity continuum (IPCM, Isodensity Polarizable Continuum Model) showed the S_6 structure to have a higher energy than the T_h structure (Jarzecki et al., 2004). It should be noted that the tilting and rotation have only a modest effect on the Fe-O stretching and bending vibrational frequencies, which are the main determinants of equilibrium isotope fractionation. Therefore, these artifacts are of minor consequence for the present study.

3.1.2. $Fe(H_2O)_6^{2+}$

Unlike the ferric complex, modeling of $Fe(H_2O)_6^{2+}$ required symmetry lowering to C_i, even in vacuo, due to the Jahn-Teller effect; Fe^{2+} has a d^6 electron configuration and hence a nominally octahedral complex is subject to distortion because one of the three d_π orbitals is doubly occupied. In Table 2, bond lengths and angles for both C_i structures (with and without PCM) are compared to X-ray data for the ammonium Tutton salt, $(NH_4)_2[Fe(H_2O)_6]SO_4$ (Cotton et al., 1993).

The $Fe(H_2O)_6^{2+}$ structure computed in vacuo is an essentially tetragonal complex, with four equatorial bonds of length 2.14 Å and two axial bonds of length 2.11 Å. The observed bond lengths in the salt are almost exactly the same (2.14 Å and 2.10 Å). The bond length differences are small, since the the d_π orbitals are essentially nonbonding. The differences are much larger, ~0.25 Å, for $Cr(H_2O)_6^{2+}$ and $Cu(H_2O)_6^{2+}$, which have an extra electron in one of the two antibonding d_σ orbitals (Cotton et al., 1993). As with $Fe(H_2O)_6^{3+}$, application of the PCM model decreases the Fe-O distances by 0.015 to 0.03 Å. In this case PCM slightly worsens the agreement with experiment (by up to 0.03 Å).

All other predicted bond lengths, and all bond angles, show excellent agreement with the salt data, where available. C_i symmetry permits tilting and rotation of the water molecules. This effect was small in vacuo, but increased substantially in the PCM model. Data on water tilt and rotation are not available, but substantially enhanced distortions in the PCM model, as in the case of the ferric complex, are likely to be PCM artifacts (Jarzecki et al., 2004).

3.2. Molecular Vibrations

We are interested here in a subset of all possible vibrational modes of $Fe(H_2O)_6^{2+}$ and $Fe(H_2O)_6^{3+}$, those sensitive to Fe isotope substitution of the central atom. These modes are necessarily IR active. For detailed discussion of DFT results for other vibrational modes (i.e., Raman-active vibrations), the reader is referred to Jarzecki et al. (2004). The calculated symmetry modes and IR frequencies of these vibrations for various model cases, and their sensitivities to isotope substitution, are summarized in Table 3 along with computed IR intensities.

For comparison with DFT predictions, Table 3 also includes the available IR spectroscopic data. Infrared spectra have been reported for polycrystalline samples of $Fe(H_2O)_6^{3+}$ alums (Best et al., 1980) and of $Fe(H_2O)_6^{2+}$ in SiF_6^{2-} salt (Nakagawa and Simanouchi, 1964). IR assignments were based on trends among hexa-aquo ions, and for $Fe(H_2O)_6^{3+}$, on measured $^{50/53}Cr$ isotope shifts in the chromium alum. These data were used as input to previous MUBFF models (Schauble et al., 2001).

3.2.1. Vibrational modes

In the absence of Jahn-Teller distortion and rotation or tilting of the water ligand molecules, the vibrational modes of

Table 3. Calculated vibrational frequencies ($^{56}\nu$; cm^{-1}), isotope shifts ($^{56}\nu/^{54}\nu$) and IR intensities (km/mol) for DFT and DFT-PCM models of $Fe(H_2O)_6^{3+}$ and $Fe(H_2O)_6^{2+}$. Experimental frequencies are given where available.

IR Vibrational Assignment	$Fe(H_2O)_6^{3+}$						$Fe(H_2O)_6^{2+}$					
	DFT (T_h)[†]		DFT-PCM (S_6)[‡]			Expt.[b]	DFT (C_i)[†]		DFT-PCM (C_i)[a,‡]			Expt.[c]
	$^{56}\nu$	$^{56}\nu/^{54}\nu$	$^{56}\nu$	$^{56}\nu/^{54}\nu$	IR int.	$^{56}\nu$	$^{56}\nu$	$^{56}\nu/^{54}\nu$	$^{56}\nu$	$^{56}\nu/^{54}\nu$	IR int.	$^{56}\nu$
O-Fe-O def (ν_6; T_{2u})	127 (T_u)	0.99992	108 (A_u)	0.99982	7		90	0.99933	79	1.00000	69	
	127 (T_u)	0.99992	112 (E_u)	0.99982	74		98	0.99959	86	0.99919	34	
	127 (T_u)	0.99992	112 (E_u)	0.99982	74		104	0.99990	107	0.99888	45	
O-Fe-O def (ν_4; T_{1u})	185 (T_u)	0.99456	164 (A_u)	0.99491	7		121	0.99530	124	0.99728	138	
	185 (T_u)	0.99456	188 (E_u)	0.99466	28	304[d]	135	0.99526	133	0.99564	27	
	185 (T_u)	0.99456	188 (E_u)	0.99466	28		137	0.99543	170	0.99567	169	
Fe-O stretch (ν_3; T_{1u})	434 (T_u)	0.99498	470 (E_u)	0.99441	77		340	0.99532	363	0.99539	205	389
	434 (T_u)	0.99498	470 (E_u)	0.99441	77		373	0.99733	386	0.99512	77	
	434 (T_u)	0.99498	487 (A_u)	0.99389	304	505	387	0.99793	388	0.99403	106	
H_2O twist	257 (E_u)	1.00000	225 (E_u)	0.99978	286		189	0.99979	242	0.99996	214	
	257 (E_u)	1.00000	225 (E_u)	0.99978	286		243	0.99959	266	0.99996	80	
	478 (A_u)	1.00000	293 (A_u)	0.99980	4		421	0.99969	331	0.99970	113	
H_2O wag (out-of-plane)	532 (T_u)	0.99976	304 (E_u)	0.99957	1121		319	0.99713	137	0.99738	360	
	532 (T_u)	0.99976	304 (E_u)	0.99957	1121		345	0.99653	413	0.99802	653	(*)[e]
	532 (T_u)	0.99976	359 (A_u)	0.99909	149		403	0.99888	470	0.99974	598	
H_2O rock (in plane)	672 (T_u)	0.99877	769 (E_u)	0.99973	275		538	0.99883	518	0.99873	332	575
	672 (T_u)	0.99877	769 (E_u)	0.99973	275	668	563	0.99874	605	0.99955	133	
	672 (T_u)	0.99877	774 (A_u)	0.99970	164		565	0.99887	681	0.99968	201	

[a] All vibrations are of A_u symmetry;
[b] IR bands observed in cesium alums (Best et al., 1980).
[c] IR bands observed in $FeSiF_6 \cdot 6H_2O$ (Nakagawa and Simanouchi, 1964).
[d] This mode is suggested to have a substantial contribution from the wagging coordinate because of its considerable IR intensity.
[e] Observed by a very strong band of SiF_6^{2-} at 485 cm^{-1} (Nakagawa and Simanouchi, 1964
[†] B3LYP/6-31G* & Ahlrichs' VTZ level of theory (in vacuo).
[‡] PCM B3LYP/6-31G* & Ahlrichs' VTZ level of theory in PCM ($\varepsilon = 78.4$).

$Fe(H_2O)_6^{3+}$ in vacuo can be classified among the symmetry species of T_h symmetry as follows:

$$\Gamma = 8\ T_u + 5\ T_g + 1\ E_u + 3\ E_g + 1\ A_u + 1\ A_g$$

Among these, only the T_u modes are IR active and potentially Fe-isotope sensitive, and hence, significant for estimations of equilibrium Fe-isotope fractionations (the T_g, E_g, and A_g modes appear only in Raman spectra, and the A_u and E_u modes are silent in both spectra). Three of these modes do not couple with the metal center, and are, therefore, not Fe-isotope sensitive. These are two symmetric and antisymmetric O-H stretching modes and H_2O scissors vibrations, all of which occur at frequencies >1000 cm^{-1}. The remaining 5 T_u bands, all Fe-isotope sensitive and triply degenerate, correspond to H_2O rocking, H_2O wagging, Fe-O stretching, and two O-Fe-O deformations.

As noted above, when PCM is applied to $Fe(H_2O)_6^{3+}$, H_2O rotation and tilting must be allowed, which results in an optimal S_6 structure. In this case the T_u triple degeneracies are lifted, yielding doubly degenerate E_u and split A_u modes that are all sensitive to isotope substitution. This includes the E_u and A_u modes associated with the H_2O twist. These modes only couple with the central atom as a result of the distortion of the H_2O orientation in this symmetry group.

For $Fe(H_2O)_6^{2+}$, which has a C_i structure both in vacuo and under PCM, all modes are Fe-isotope sensitive and nondegenerate. Large frequency splits are computed for each mode type. The splits are especially large under the influence of the PCM, which induces large differences among the tilt and rotation coordinates of the water molecules (Table 2).

3.2.2. *Vibrational frequencies*

Comparison of predicted vibrational frequencies with available IR data reveals good agreement, but also some surprises. The predicted Fe-O stretching bands are in accord with observations (Table 3). For both complexes, the predicted frequencies fall in the 300 to 500 cm^{-1} region and shift up significantly when the PCM is applied, reflecting shorting of the Fe-O bonds (Tables 1 and 2). Predicted frequencies are higher for $Fe(H_2O)_6^{3+}$ than for $Fe(H_2O)_6^{2+}$, also as expected from Fe-O bond lengths. Experimental frequencies are 505 cm^{-1} and 389 cm^{-1} for $Fe(H_2O)_6^{3+}$ and $Fe(H_2O)_6^{2+}$, respectively, vs. theoretical values of 470 to 487 cm^{-1} and 363 to 388 cm^{-1} for the respective PCM models. The experimental values are well within the nominal $\pm$ 25 cm^{-1} uncertainties of the PCM predicted frequencies. Agreement is slightly worse for the respective in vacuo models, which predict frequencies of 434 cm^{-1} and 340 to 387 cm^{-1}.

Agreement between theory and experiment is also reasonable, but not as good, for the H_2O rocking mode. Discrepancies are as large as ~100 cm^{-1} for both complexes. However, the experimental water modes are difficult to assign and the PCM artifacts noted above may be important. Additionally, because little energy is associated with rotation and tilting of the H_2O molecules, it is at least plausible that the orientations of these molecules differ between the models and $Fe(H_2O)_6^{3+}$ alums and

$Fe(H_2O)_6^{2+}$ in SiF_6^{-2} salt, affecting the frequencies of the water librational modes. Importantly, because these modes have relatively little sensitivity to Fe isotope substitution, this discrepancy is of minor importance for isotope fractionation predictions.

Observed Raman spectra and DFT predictions, discussed in Jarzecki et al. (2004), are also reasonably close. Fe-O stretching is particularly important because it directly reflects Fe-O bond strength. The Raman frequency for this stretch in aqueous solution is reported by Kanno (1988) as 510 cm^{-1} and 380 cm^{-1} for the Fe^{3+} and Fe^{2+} complexes, respectively. The respective DFT-PCM predictions for the ν_1 vibration for the solvated complexes are 486 cm^{-1} and 392 cm^{-1}. Although this mode is not isotope sensitive, this broad agreement of theory and experiments increases confidence in the DFT models.

In contrast to these favorable comparisons, there is a discrepancy of as much as 136 cm^{-1} between theory and experiment for the O-Fe-O bending mode of $Fe(H_2O)_6^{3+}$ (no ν_4 band has been reported for $Fe(H_2O)_6^{2+}$). What is the source of this large discrepancy? We considered the possibility of basis set dependence of the computed results, or dependence on the level of theory. However, trial calculations with extra diffuse and polarization functions on Fe, O, and H produced only small changes in the mode frequencies, as did switching to a different density functional, B3PW91.

Experience has shown that DFT derived mode frequencies are reasonably close to experimental values, but deviations are sometimes encountered that reflect neglect of anharmonicity, basis set errors, and medium effects. With sufficient data, these can be corrected by scaling the force constants empirically. Pulay and coworkers have shown that a limited set of scaling factors can successfully reproduce experimental spectra for many classes of molecules, including metal complexes (e.g., Kozlowski et al., 1996a; Kozlowski et al., 1996b; Jarzecki et al., 1997; Kozlowski et al., 1999; Diaz-Acosta et al., 2001; Diaz-Acosta et al., 2003). In the present case, however, the data are limited. We tried applying the scaling factors developed for metal acetylacetonates (Diaz-Acosta et al., 2001), but found that our computed frequencies were altered very little because of compensation among the factors, some of which are higher and some lower than unity. Because Pulay and coworkers obtained accurate mode frequencies for the metal acetylacetonates, including the bending modes, it seems unlikely that DFT would fail for hexa-aquo complexes.

We suggest instead that the DFT predictions are fairly accurate and that the discrepancy is attributable to one of two alternatives that relate to the experimental data.

First, it is at least conceivable that the prior assignment of the 304 cm^{-1} IR feature to ν_3 is incorrect. We note that the DFT model predicts that the H_2O wagging mode should appear at this frequency, and that this is expected to be an intense absorption feature.

Second, this feature, correctly assigned, might be strongly shifted due to the effects of crystal forces on the experimental mode frequencies. Although application of PCM to the in vacuo calculation introduces polarization effects representative of liquid water, the effects of directional H-bonds are not included. These are clearly revealed in the alum neutron structures of $Fe(H_2O)_6^{3+}$ (Best and Forsyth, 1990), and are no doubt present in $Fe(H_2O)_6(SiF_6)$ as well. H-bonds are expected to alter the potential surface of the complexes, especially with respect to the O-Fe-O bending coordinates. The directional H-bonds anchor the water molecule and raise the effective force constants for O-Fe-O bending. In this respect, the DFT computation may be more representative of the aquo ions in solution than in the crystals; although H-bonds also form with solvent molecules, they are not rigid anchors as in the crystals. The proposal that lattice forces elevate the bending frequencies is supported by the previous finding that the ν_5 (Raman active) doublet of $Fe(H_2O)_6(SiF_6)$, seen at 210/231 cm^{-1} at 15 K,

Table 4. Reduced partition function ratios, $10^3 \cdot \ln(\beta_{56-54})$, and equilibrium fractionation factors, $10^3 \cdot \ln(\alpha)$, for $Fe(H_2O)_6^{3+}$ and $Fe(H_2O)_6^{2+}$ calculated using DFT-PCM, DFT, and MUBFF models between 0 and 300°C.

	DFT-PCM[a]			DFT[b]			MUBFF[c]		
	$10^3 \cdot \ln(\beta_{56-54})$			$10^3 \cdot \ln(\beta_{56-54})$			$10^3 \cdot \ln(\beta_{56-54})$		
T (°C)	$Fe(H_2O)_6^{3+}$	$Fe(H_2O)_6^{2+}$	$10^3 \cdot \ln(\alpha)$	$Fe(H_2O)_6^{3+}$	$Fe(H_2O)_6^{2+}$	$10^3 \cdot \ln(\alpha)$	$Fe(H_2O)_6^{3+}$	$Fe(H_2O)_6^{2+}$	$10^3 \cdot \ln(\alpha)$
0	10.73	7.88	2.85	11.09	7.71	3.38	13.59	7.35	6.24
10	10.04	7.37	2.68	10.39	7.21	3.18	12.72	6.87	5.85
20	9.42	6.90	2.52	9.75	6.76	2.99	11.93	6.43	5.50
22	9.30	6.82	2.48	9.63	6.68	2.95	11.78	6.35	5.43
25	9.13	6.69	2.44	9.45	6.55	2.90	11.56	6.23	5.33
30	8.86	6.48	2.37	9.17	6.36	2.81	11.20	6.03	5.17
40	8.34	6.10	2.24	8.64	5.98	2.65	10.54	5.67	4.87
50	7.86	5.75	2.12	8.15	5.64	2.51	9.93	5.34	4.59
60	7.43	5.42	2.00	7.70	5.33	2.37	9.38	5.04	4.34
70	7.03	5.13	1.90	7.29	5.04	2.24	8.87	4.76	4.10
80	6.66	4.85	1.80	6.91	4.78	2.13	8.40	4.51	3.89
90	6.31	4.60	1.71	6.56	4.54	2.02	7.96	4.27	3.69
100	6.00	4.37	1.63	6.23	4.31	1.92	7.56	4.06	5.17
200	3.81	2.76	1.05	3.97	2.76	1.21	4.77	2.57	2.20
300	2.61	1.90	0.72	2.75	1.93	0.82	3.26	1.77	1.49

[a] PCM B3LYP/6-31G* and Ahlrichs' VTZ level of theory in PCM ($\varepsilon = 78.4$).
[b] B3LYP/6-31G* & Ahlrichs' VTZ level of theory (in vacuo).
[c] MUBFF following Schauble et al. (2001).

shifted down to 187/198 cm^{-1} at 300 K (Jenkins and Lewis, 1981). At the same time, a shift of low-frequency lattice modes signaled a phase change at low temperature. We suggest that the high-temperature phase allows greater mobility of the bound water molecules, as signaled by diminished O-Fe-O bending frequencies.

Although the bending modes are most sensitive to the presence of directional H-bonds, it is plausible that the Fe-O stretching modes are also somewhat affected, and that the smaller, but still sizable, discrepancies between observed and computed frequencies of these modes can be similarly understood.

3.2.3. *Vibrational isotope sensitivity*

In the case of idealized O_h symmetry, assumed in MUBFF treatments, only two vibrational modes are sensitive to isotope substitution, ν_3 and ν_4. The situation is clearly different in the symmetries simulated by DFT. Although the Fe-O stretches and bends are clearly distinguishable from the water librational modes, there is some mixing of the coordinates, and hence, the DFT model spreads the isotope shifts into asymmetrical water librational modes, as well as the Fe-O stretches and bends. This can be seen in the small but nonneglegible Fe isotope shifts calculated for the water modes (Table 3), especially the wagging and rocking modes. For $Fe(H_2O)_6^{2+}$, the shifts associated with the wagging modes are almost as large as those of the Fe-O stretches in the in vacuo computation, and about half as large in the PCM model. We observe that the product of all the isotope frequency ratios is the same for the two computations (MUBFF vs. DFT), consistent with the Redlich-Teller product rule (Wilson et al., 1955).

3.3. Isotope Fractionation

3.3.1. *Comparison of predicted reduced partition functions*

Reduced partition function ratios for $Fe(H_2O)_6^{2+}$ and $Fe(H_2O)_6^{3+}$ over a range of temperatures, calculated from Eqn. 3 using DFT vibrational frequencies (in vacuo and with PCM; Table 3), are presented in Table 4 and Figure 3 (note that calculated temperature dependence considers only the temperature dependence of Q_{vib}; more complicated effects, such as change in solvent polarizabily with T, are not considered). Also shown are MUBFF results, calculated from Eqn. 3 using the MUBFF derived isotope frequency shifts of Schauble et al. (2001). These shifts were obtained using the experimental Fe-O stretching and O-Fe-O bending frequencies reported in Table 5 ($Fe(H_2O)_6^{3+}$: ν_3 = 505 cm^{-1}; ν_4 = 304 $\chi\mu^{-1}$; $Fe(H_2O)_6^{2+}$: ν_3 = 389 cm^{-1}) and an estimated bending frequency for $Fe(H_2O)_6^{2+}$ (ν_4 = 195 cm^{-1}) (Schauble et al., 2001). For both DFT and MUBFF model results, we also tabulate $10^3 \cdot \ln(\alpha)$.

A counterintuitive feature of the DFT results requires explanation: the slight decrease of $10^3 \cdot \ln(\beta_{56-54})$ predicted for the Fe^{3+} complex in the DFT-PCM model as compared to in vacuo. The result is unexpected because solvation should stabilize the complex, increasing the effective force constants acting on the Fe atom, and hence, the tendency to concentrate heavy isotopes. Why then, is the reduced partition function of the DFT-PCM model smaller than computed in vacuo? The answer lies in the competition between solvation stabilization and the breakage of T_h to S_6 symmetry in the optimized PCM. The symmetry breaking activates new u-symmetry bands, which decreases the reduced partition function ratios. The relative importance of these effects can be illustrated by some test calculations. Using the PCM frequencies for only two major modes, ν_3 and ν_4, the predicted $10^3 \cdot \ln(\beta_{56-54})$ at 22°C increases from 9.63 in vacuo to 13.16 in solution, as intuitively expected. However, when using all the Fe-sensitive bands predicted for the distorted solvated complex, the predicted $10^3 \cdot \ln(\beta_{56-54})$ *decreases* to 5.78. This effect is unimportant for the Fe^{2+} complex because its symmetry is not broken by solvation.

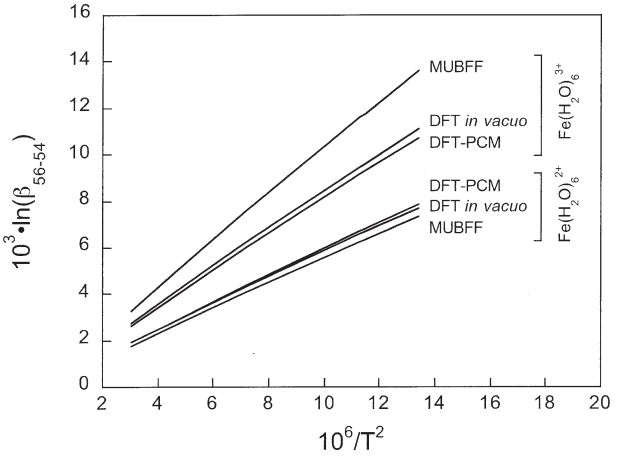

Fig. 3. Reduced partition function ratios, $10^3 \cdot \ln(\beta_{56-54})$, for $Fe(H_2O)_6^{3+}$ and $Fe(H_2O)_6^{2+}$ vs. temperature (~ 273–700 Kelvin), calculated using MUBFF, DFT (in vacuo), and DFT-PCM models as described in the text. DFT-based models lead to substantial downward revision of $Fe(H_2O)_6^{3+}$ values.

Comparison of DFT and MUBFF model results shows good qualitative agreement. In both cases, $10^3 \cdot \ln(\alpha) \sim 1$–5 is predicted between the complexes. This fractionation increases about fourfold as temperature decreases from 300 to 0°C (Table 4). Preferential partitioning of ^{56}Fe in $Fe(H_2O)_6^{3+}$ is predicted, consistent with the rule-of-thumb that the heavier isotope should prefer the stronger bonding environment (e.g., Criss, 1999).

However, substantial quantitative differences are apparent between the DFT and MUBFF estimates of $10^3 \cdot \ln(\beta_{56-54})$ for $Fe(H_2O)_6^{3+}$ (Fig. 3). As a result, the $10^3 \cdot \ln(\alpha)$ values predicted by MUBFF are roughly twice the magnitude of the DFT predictions with PCM (Table 4; Fig. 4). For example, at 22°C, DFT-PCM predicts $10^3 \cdot \ln(\alpha) \sim 2.5$, whereas MUBFF predicts $10^3 \cdot \ln(\alpha) \sim 5.4$. This difference is substantially larger than the difference between the $10^3 \cdot \ln(\alpha)$ predictions of the in vacuo and DFT-PCM models ($10^3 \cdot \ln(\alpha_{vacuo})$ - $10^3 \cdot \ln(\alpha_{PCM}) \sim 0.5$), which agree to within 20% of each other.

Why are the MUBFF and DFT results so discordant? There are two primary factors: first, the frequencies used to obtain β_{56-54} in the two calculations are substantially different; and second, the DFT models spread the isotope shifts into asymmetrical water librational modes, as well as the Fe-O stretches and bends.

The frequency differences account for most of the discrepancy. This can be demonstrated by retaining the MUBFF isotope frequency ratios ($^{56}\nu_3/^{54}\nu_3$ = 0.9943 and $^{56}\nu_4/^{54}\nu_4$

Table 5. Reduced partition function ratios, $10^3 \cdot \ln(\beta_{56-54})$, and equilibrium fractionation factors, $10^3 \cdot \ln(\alpha)$, between 0 and 300°C for $Fe(H_2O)_6^{3+}$, and $Fe(H_2O)_6^{2+}$ calculated using MUBFF models modified with DFT-PCM frequencies (see text).

	MUBFF w/DFT-PCM ν_3, ν_4			MUBFF w/DFT-PCM ν_4 ($Fe(H_2O)_6^{3+}$)		
	$10^3 \cdot \ln(\beta_{56-54})$			$10^3 \cdot \ln(\beta_{56-54})$		
T (°C)	$Fe(H_2O)_6^{3+}$	$Fe(H_2O)_6^{2+}$	$10^3 \cdot \ln(\alpha)$	$Fe(H_2O)_6^{3+}$	$Fe(H_2O)_6^{2+}$	$10^3 \cdot \ln(\alpha)$
0	10.30	6.73	3.57	11.48	See DFT-PCM (Table 4)	4.13
22	8.91	5.81	3.10	9.97		3.62
25	8.75	5.69	3.06	9.79		3.56
100	5.71	3.69	2.02	6.46		2.40
200	3.60	2.31	1.29	4.13		1.56
300	2.47	1.58	0.89	2.87		1.10

= 0.9937 for $Fe(H_2O)_6^{3+}$, and 0.9937 and 0.9943 for $Fe(H_2O)_6^{2+}$; Schauble et al., 2001), and changing the frequencies to those computed by DFT (averages of the three components; Table 3): 475 and 180 cm^{-1} for ν_3 and ν_4 of $Fe(H_2O)_6^{3+}$, and 379 and 142 cm^{-1} for ν_3 and ν_4 of $Fe(H_2O)_6^{2+}$. The result of this "ν_3, ν_4 corrected" MUBFF calculation is $10^3 \cdot \ln(\alpha) \sim 3.1$ at 22°C (Table 5). Thus 80% of the difference with respect to the DFT-PCM treatment is due to the difference in frequencies. The remainder is attributable to the spreading of the isotope shifts across other vibrational modes.

In fact, most of the difference is attributable to a single discrepant bending frequency, ν_4, of $Fe(H_2O)_6^{3+}$. As discussed above, the DFT-computed frequency is much lower than the assignment from the observed band in the alum spectrum. If all MUBFF frequencies are retained except for ν_4 of $Fe(H_2O)_6^{3+}$, then $10^3 \cdot \ln(\alpha) \sim 3.6$ at 22°C (Table 5). Thus, lowering this one frequency moves the predicted fractionation ~ 2/3 of the way to the DFT-PCM value. This explains why large disagreement is seen in the predicted $10^3 \cdot \ln(\beta_{56-54})$ values of $Fe(H_2O)_6^{3+}$ while good agreement is seen for $Fe(H_2O)_6^{2+}$.

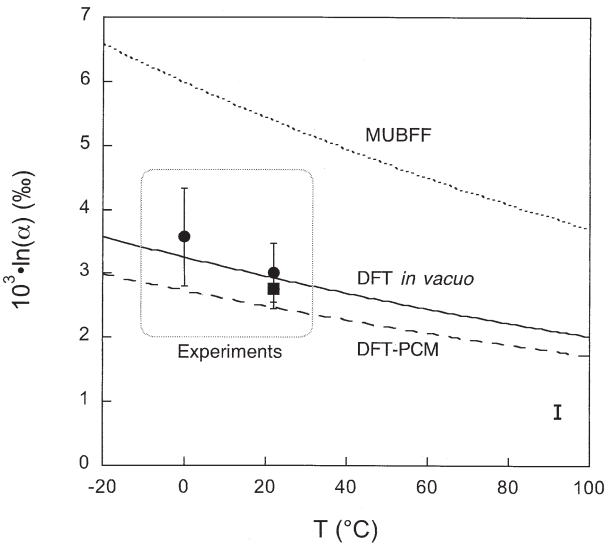

Fig. 4. Comparison of the equilibrium fractionation factor, $10^3 \cdot \ln(\alpha)$, between $Fe(H_2O)_6^{3+}$ and $Fe(H_2O)_6^{2+}$ computed using MUBFF, DFT (in vacuo), and DFT-PCM models over the temperature range 0 to 100°C. Fractionation predicted using DFT-PCM is substantially smaller than using MUBFF. Also shown are determinations of this fractionation factor from mass spectrometric experiments at 0°C and 22°C (squares: Johnson et al., 2002; circles: Welch et al., 2003). Representative uncertainty on DFT results is indicated in the lower right.

3.3.2. *Comparisons with mass spectrometric data*

The DFT and MUBFF results for $10^3 \cdot \ln(\alpha)$ are compared to results from mass spectrometric studies of Fe isotope fractionation between $Fe(H_2O)_6^{3+}$ and $Fe(H_2O)_6^{2+}$ in experimental systems in Table 6 (Johnson et al., 2002; Welch et al., 2003). The most refined experimental study reports $10^3 \cdot \ln(\alpha)$ 3.57 ± 0.76 at 0°C and 3.00 ± 0.46 at 22°C. This compares favorably to predictions of 3.38 and 2.95 at these temperatures from DFT in vacuo, and 2.85 and 2.48 from DFT-PCM. The in vacuo results

Table 6. Expected fractionation of $^{56}Fe/^{54}Fe$ between $Fe(H_2O)_6^{3+}$ $-Fe(H_2O)_6^{2+}$ at equilibrium ($\Delta = 10^3 \cdot \ln(\alpha)$), T = 0–300°C. Experimentally constrained fractionations are also given. Results for temperatures at which direct experimental measurements are available are **highlighted.**

	Δ ($Fe(H_2O)_6^{3+} - Fe(H_2O)_6^{2+}$) (‰)			
T (°C)	DFT-PCM[a]	DFT[b]	MUBFP[c]	Experimental[d]
0	**2.85**	**3.38**	6.24	**3.60 (3.57)**
10	2.68	3.18	5.85	3.29
20	2.52	2.99	5.50	3.01
22	**2.48**	**2.95**	**5.43**	**2.96 (3.00)**
25	2.44	2.90	5.33	2.88
30	2.37	2.81	5.17	2.76
40	2.24	2.65	4.87	2.53
50	2.12	2.51	4.59	2.32
60	2.00	2.37	4.34	2.13
70	1.90	2.24	4.10	1.96
80	1.80	2.13	3.89	1.80
90	1.71	2.02	3.69	1.65
100	1.63	1.92	5.17	1.52
200	1.05	1.21	2.20	0.61
300	0.72	0.82	1.49	0.14

[a] PCM B3LYP/6-31G* & Ahlrichs' VTZ level of theory in PCM (ε = 78.4).
[b] B3LYP/6-31G* & Ahlrichs' VTZ level of theory (in vacuo).
[c] MUBFF following Schauble et al. (2001).
[d] From empirical fit to experimental data, $10^3 \cdot \ln(\alpha) = ([0.334 \pm 0.032] \times 10^6)/T^2 - 0.88 \pm 0.38$, T in Kelvin (Welch et al. 2003). Direct measurements indicated in parenthesis. Experimental ± 2σ uncertainties are ±0.5–0.6 for direct measurements and ±1.0–1.5 for empirical function. Experimental $10^3 \cdot \ln(\alpha)$ = 3.00 ± 0.46 at 22°C supercedes previous value of 2.75 ± 0.30 (Johnson et al., 2002).

are well within the $\pm 2\sigma$ analytical uncertainties, while the DFT-PCM results are just outside these uncertainties.

The DFT and MUBFF results are compared to mass spectrometric measurements of Fe isotope fractionation as a function of temperature in Figure 4, and to predictions from the experimentally constrained function of Welch et al. (2003) in Table 6. The DFT temperature-dependent trends are in reasonable agreement with direct experimental determinations, although the experimental dataset is limited. This finding provides some confidence in the use of theoretical temperature functionality to extrapolate to T > 22°C. Deviations from the empirical T function are most apparent at high temperatures. Theoretical temperature dependence could be more reliable than the empirical function because the latter was derived from a fit to data at only two temperatures (0°C and 22°C). Further experimental work is needed to test this possibility.

The small (<0.5 ‰) offset between the most probable experimental values (i.e., the values at the center of uncertainty estimates) and DFT-PCM results suggests that there is some remaining inaccuracy in either the models or the experimental data. DFT-PCM should be superior to the DFT in vacuo model, and in fact better matches vibrational data (Table 3). Hence, we regard as fortuitous the apparent superiority of DFT in vacuo vs. DFT-PCM in matching the experimental results. However, the PCM does not account for H-bonding, the effects of other dissolved ions (such as Cl^-), or pH (experiments were conducted at pH < 7), and as noted above, the level of PCM modeling used here is not free from artifacts. One or all of these factors could account for the discrepancy.

At the same time, it must be noted that the experimental data are corrected for isotope shifts of ~ 0.2‰ resulting from partial reequilibration that occurs during separation of the two complexes (Johnson et al., 2002; Welch et al., 2003). Adjustment of this correction accounts for the difference between the two experimental determinations at 22°C. It is possible that this correction is slightly inaccurate, or that other small experimental artifacts are as yet unrecognized.

3.3.3. Dissolved Fe-mineral fractionation

The DFT results can be used to revise calculations of Fe isotope equilibrium fractionation between dissolved and mineral-bound Fe. These fractionations were previously calculated by Skulan et al. (2002) using $10^3 \cdot \ln(\beta_{56-54})$ results from the MUBFF study of Schauble et al. (2001) for aqueous species and from the Mössbauer study of Polyakov and Mineev (2000) for Fe-bearing minerals. Disagreement between theoretical and mass spectrometric determinations of the fractionation between dissolved Fe^{3+} and hematite (Fe_2O_3) led to tentative questioning of the MUBFF derived $10^3 \cdot \ln(\beta_{56-54})$ for $Fe(H_2O)_6^{3+}$ (Skulan et al., 2002).

Expected fractionation between $Fe(H_2O)_6^{3+}$ and hematite using DFT-PCM results is shown in Figure 5, along with predictions of fractionations between $Fe(H_2O)_6^{3+}$ and goethite (α-FeOOH) and magnetite (Fe_3O_4). MUBFF-based predictions are shown for comparison. In all cases, $10^3 \cdot \ln(\alpha) = 10^3 \cdot \ln(\beta_{56-54}(Fe(H_2O)_6^{3+})) - 10^3 \cdot \ln(\beta_{56-54}(\text{mineral}))$, with $10^3 \cdot \ln(\beta_{56-54}(Fe(H_2O)_6^{3+}))$ obtained from DFT-PCM or MUBFF models and $10^3 \cdot \ln(\beta_{56-54}(\text{mineral}))$ from Mossbauer-based theory (Polyakov and Mineev, 2000). Unlike hematite and goethite, magnetite contains two types of crystallographically distinct Fe sites: tetrahedral "A" sites and octahedral "B" sites, in a 1:2 ratio. Mössbauer-based estimates of $10^3 \cdot \ln(\beta_{56-54})$ for both types of sites are available (Polyakov and Mineev, 2000). Hence, we assumed $10^3 \cdot \ln(\beta_{56-54}(Fe_3O_4)) = [10^3 \cdot \ln(\beta_{56-54}(Fe_3O_4\text{-A})) + 2 \cdot 10^3 \cdot \ln(\beta_{56-54}(Fe_3O_4\text{-B}))]/3$.

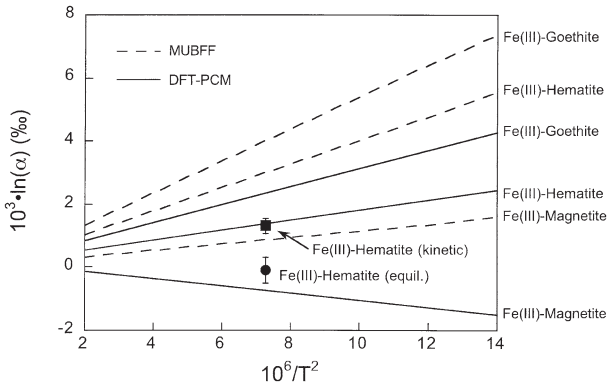

Fig. 5. Estimated equilibrium fractionation factors, $10^3 \cdot \ln(\alpha)$, between $Fe(H_2O)_6^{3+}$ (Fe(III)) and goethite, hematite and magnetite over the temperature range 273 to ~ 700 Kelvin. Calculations computed using Mossbauer derived $10^3 \cdot \ln(\beta_{56-54})$ for minerals (Polyakov and Mineev, 2000) and $10^3 \cdot \ln(\beta_{56-54})$ for $Fe(H_2O)_6^{3+}$ derived from MUBFF or DFT-PCM methods (see text). Fractionations predicted using DFT-PCM are substantially smaller than using MUBFF. Also shown is the Fe(III)-hematite equilibrium fractionation factor determined from mass spectrometric experiments and the kinetic fractionation seen during rapid precipitation of hematite from dissolved ferric Fe (Skulan et al., 2002).

It is apparent that with DFT-PCM, expected fractionations are reduced by about a factor of two as compared to MUBFF results (Fig. 5). Therefore, as with the fractionation between $Fe(H_2O)_6^{3+}$ and $Fe(H_2O)_6^{2+}$, DFT brings theory closer to agreement with mass spectrometric determinations in the case of Fe^{3+}-hematite (the only system for which a mass spectrometric determination is available). However, unlike fractionation between $Fe(H_2O)_6^{3+}$ and $Fe(H_2O)_6^{2+}$, a sizeable discrepancy of nearly 1.5 ‰ remains.

The reason for this residual disagreement is unclear. It probably does not reflect inaccuracy in the DFT-PCM results, in view of the $Fe(H_2O)_6^{3+}$ and $Fe(H_2O)_6^{2+}$ results discussed above (Fig. 4). It could indicate an unrecognized inaccuracy in the Mössbauer derived $10^3 \cdot \ln(\beta_{56-54})$, or in experiments. It is intriguing that the predicted effect is very similar to the ~ –1 ‰ kinetic isotope effect reported during precipitation of hematite from ferric solution, but this agreement may be fortuitous.

4. CONCLUSIONS & IMPLICATIONS

This study resolves the disagreement between theoretical and experimental determinations of the fractionation factor between $Fe(H_2O)_6^{3+}$ and $Fe(H_2O)_6^{2+}$, effectively validating mass spectrometric determinations of $10^3 \cdot \ln(\alpha) \sim 3$ (Johnson et al., 2002; Welch et al., 2003).

More broadly, our analysis of this system illustrates the value of modern computational chemistry methods for prediction of Fe isotope effects and, by extension, heavy stable isotope

effects in general. The use of DFT-based models to obtain vibrational frequencies a priori is seen to be particularly important when published IR spectra are of metals in salts or other materials in which vibrational motions may not be representative of the free complexes in solution (or in vacuo). This is a more serious problem for aqueous complexes than gaseous molecules. Therefore it is a more critical problem for heavy elements where gases are essentially irrelevant in nature, as compared to traditional light stable isotopes. For these reasons, further work with DFT or other ab initio approaches will be critical in the development of heavy stable isotope geochemistry.

Although not emphasized in this study, DFT and ab initio methods are the only reliable route for prediction of isotope effects involving mixed-ligand complexes (e.g., $Fe(H_2O)_5Cl^{2+}$, $Fe(H_2O)_5OH^{2+}$) because such complexes cannot be idealized to octahedral or tetrahedral symmetry as required by MUBFF methods. This is an important area for future work because such species are important in natural waters (especially seawater) and when pH > 5, and have been implicated in Fe isotope fractionation in natural and experimental systems (e.g., Anbar et al., 2000; Bullen et al., 2001; Roe et al., 2003). It will also be important to assess the effects of pH and ionic strength on vibrational frequencies in future theoretical work, another area where the utility of MUBFF is limited.

At the same time, our analysis indicates that MUBFF models are not unreasonable for the prediction of isotope effects if accurate experimental frequencies are available for the vibrational modes with greatest isotope sensitivity. This conclusion is similar to that reached by Schauble et al. (2001) from his comparison of observed and MUBFF-predicted isotope frequency shifts for a number of octahedral and tetrahedral species. Thus, existing MUBFF fractionation predictions for octahedral and tetrahedral Fe complexes with Cl^-, Br^-, and CN^- are not rendered irrelevant by the present study, although reexamination of these systems with DFT is recommended.

As for measurements of Fe isotope variations in the geologic record, our findings help to explain the restricted range of Fe isotope variation in BIF, where only sulfide minerals show variability significantly larger than 3‰ (Johnson et al., 2003a). However, we caution that the Fe(III)-hematite and Fe(III)-magnetite equilibrium fractionations predicted here are substantially larger than the "preferred" values inferred from measurements of natural mineral assemblages in BIF (Johnson et al., 2003a). In addition to the persistence of predicted Fe(III)-hematite fractionation despite our downward revision of $10^3 \cdot \ln(\beta_{56-54}(Fe(H_2O)_6^{3+}))$, an unusual and sizeable *inverse* fractionation (i.e., favoring heavy Fe in the mineral) is predicted between Fe(III) and magnetite. Experimental tests of this and other predictions in Figure 5 should be a priority. Ab initio estimates of mineral $10^3 \cdot \ln(\beta_{56-54})$ would also be useful. If significant Fe(III)-mineral effects exist, they will complicate attempts to infer the isotopic composition of ferric iron in fluids from which these minerals may have precipitated, such as Proterozoic surface seawater (Johnson et al., 2003a). In the meantime, caution is advised in the interpretation of Fe isotope signatures in complex natural systems involving mineral-fluid interactions. Inferences of biologic Fe processing in these ancient systems should be regarded as tentative.

Acknowledgments—The authors thank Pat Holland for suggesting this joint effort, the Gordon Research Conferences for providing an atmosphere conducive to collaboration, and François Morel for early encouragement. The thorough comments of Edwin Schauble and an anonymous reviewer are appreciated. Funding was provided by the Center for Environmental Bioinorganic Chemistry (NSF CHE 0221978) and by grants from the NASA Astrobiology Institute and NSF (EAR 0003565) to A. D. A.

Associate editor: J. Horita

REFERENCES

Amovilli C., Barone V., Cammi R., Cances E., Cossi M., Mennucci B., Pomelli C. S., and Tomasi J. (1999) Recent advances in the description of solvent effects with the polarizable continuum model. *Adv. in Quantum Chemistry* **32,** 227–261.

Anbar A. D. (2004) Iron stable isotopes: beyond biosignatures. *Earth and Planetary Science Letters* **217,** 223–236.

Anbar A. D., Roe J. E., Barling J., and Nealson K. H. (2000) Nonbiological fractionation of iron isotopes. *Science* **288,** 126–128.

Arnold G. L., Anbar A. D., Barling J., and Lyons T. W. (2004a) Molybenum isotope evidence for widespread anoxia in mid-Proterozoic oceans. *Science* **304,** 87–90.

Arnold G. L., Weyer S., and Anbar A. D. (2004b) Fe isotope variations in natural materials measured using high mass resolution MC-ICP-MS. *Analytical Chemistry* **76,** 322–327.

Barling J., Arnold G. L., and Anbar A. D. (2001) Natural mass-dependent variations in the isotopic composition of molybdenum. *Earth and Planetary Science Letters* **193,** 447–457.

Beard B. L. and Johnson C. M. (1999) High precision iron isotope measurements of terrestrial and lunar materials. *Geochim. Cosmochim. Acta* **63,** 1653–1660.

Beard B. L., Johnson C. M., Cox L., Sun H., Nealson K. H., and Aguilar C. (1999) Iron isotope biosignatures. *Science* **285,** 1889–1892.

Beard B. L., Johnson C. M., Skulan J. L., Nealson K. H., Cox L., and Sun H. (2003) Application of Fe isotopes to tracing the geochemical and biological cycling of Fe. *Chem. Geol.* **195,** 87–117.

Becke A. D. (1993a) Density-functional thermochemistry. 3. The role of exact exchange *J. Chem. Phys.* **98,** 5648–5652.

Becke A. D. (1993b) A new mixing of Hartree-Fock and local density-functional theories. *J. Chem. Phys.* **98,** 1372–1377.

Belshaw N. S., Zhu X. K., Guo Y., and O'Nions R. K. (2000) High precision measurement of iron isotopes by plasma source mass spectrometry. *International J. of Mass Spectrometry and Ion Processes* **197,** 191–195.

Best S. P. and Forsyth J. B. (1990) Stereochemistry of tervalent aqua ions - low-temperature neutron-diffraction structures of $CsFe(SO_4)_2$. $12H_2O$ and $CsFe(SeO_4)_2$. $12H_2O$. *J. of the Chem. Society-Dalton Transactions*, 395–400

Best S. P., Armstrong R. S., and Beattie J. K. (1980) Infrared metal-ligand vibrations of hexaaquametal(III) ions in alums. *Inorganic Chemistry* **19,** 1958–1961.

Bigeleisen J. and Mayer M. G. (1947) Calculation of equilibrium constants for isotopic exchange reactions. *J. Chem. Phys.* **15,** 261–267.

Brantley S. L., Liermann L., and Bullen T. D. (2001) Fractionation of Fe isotopes by soil microbes and organic acids. *Geol.* **29,** 535–538.

Bullen T. D., White A. F., Childs C. W., Vivit D. V., and Schulz M. S. (2001) Demonstration of significant abiotic iron isotope fractionation in nature. *Geol.* **29,** 699–702.

Bullen T. D., White A. F., and Childs C. W. (2003) Comment on "Isotopic fractionation between Fe(III) and Fe(II) in aqueous solutions" by Clark Johnson, et al. *Earth and Planetary Science Letters* **206,** 229–232.

Cammi R. and Mennucci B. (1999) Linear response theory for the polarizable continuum model. *J. Chem. Phys.* **110,** 9877–9886.

Cammi R. and Tomasi J. (1995) Remarks on the use of the apparent surface-charges (ASC) methods in solvation problems-iterative versus matrix-inversion procedures and the renormalization of the apparent charges. *J. of Computational Chemistry* **16,** 1449–1458.

Cances E., Mennucci B., and Tomasi J. (1997) A new integral equation formalism for the polarizable continuum model: Theoretical background and applications to isotropic and anisotropic dielectrics. *J. Chem. Phys.* **107,** 3032–3041.

Cossi M. and Barone V. (2001) Time-dependent density functional theory for molecules in liquid solutions. *J. Chem. Phys.* **115,** 4708–4717.

Cossi M., Barone V., Cammi R., and Tomasi J. (1996) *Ab initio* study of solvated molecules: A new implementation of the polarizable continuum model. *Chem. Physics Letters* **255,** 327–335.

Cossi M., Rega N., Scalmani G., and Barone V. (2001) Polarizable dielectric model of solvation with inclusion of charge penetration effects. *J. Chem. Phys.* **114,** 5691–5701.

Cotton F. A., Daniels L. M., Murillo C. A., and Quesada J. F. (1993) Hexaaqua dipositive ions of the 1st transition series-new and accurate structures-expected and unexpected trends. *Inorganic Chemistry* **32,** 4861–4867.

Criss R. E. (1999) *Principles of Stable Isotope Distribution.* Oxford University Press, Inc..

Diaz-Acosta I., Baker J., Cordes W., and Pulay P. (2001) Calculated and experimental geometries and infrared spectra of metal tris-acetylacetonates: Vibrational spectroscopy as a probe of molecular structure for ionic complexes. Part I *J. of Physical Chemistry A* **105,** 238–244.

Diaz-Acosta I., Baker J., Hinton J. F., and Pulay P. (2003) Calculated and experimental geometries and infrared spectra of metal tris-acetylacetonates: vibrational spectroscopy as a probe of molecular structure for ionic complexes. Part II *Spectrochimica Acta Part a-Molecular and Biomolecular Spectroscopy* **59,** 363–377.

Ditchfield R., Hehre W. J., and Pople J. A. (1971) Self-consistent molecular-orbital methods. IX. Extended Gaussian-type basis for molecular-orbital studies of organic molecules *J. Chem. Phys.* **54,** 724–728.

Ellis A. S., Johnson T. M., and Bullen T. D. (2002) Chromium isotopes and the fate of hexavalent chromium in the environment. *Science* **295,** 2060–2062.

Francl M. M., Pietro W. J., Hehre W. J., Binkley J. S., Gordon M. S., Defrees D. J., and Pople J. A. (1982) Self-consistent molecular-orbital methods. 23. A polarization-type basis set for 2nd-row elements *J. Chem. Phys.* **77,** 3654–3665.

Frisch M. J., Trucks G. W., Schlegel H. B., Scuseria G. E., Robb M. A., Cheeseman J. R., Zakrzewski V. G., Montgomery J. A., Stratmann R. E., Burant J. C., Dapprich S., Millam J. M., Daniels A. D., Kudin K. N., Strain M. C., Farkas O., Tomasi J., Barone V., Cossi M., Cammi R., Mennucci B., Pomelli C., Adamo C., Clifford S., Ochterski J., Petersson G. A., Ayala P. Y., Cui Q., Morokuma K., Malick D. K., Rabuck A. D., Raghavachari K., Foresman J. B., Cioslowski J., Ortiz J. V., Baboul A. G., Stefanov B. B., Liu G., Liashenko A., Piskorz P., Komaromi I., Gomperts R., Martin R. L., Fox D. J., Keith T., Al-Laham M. A., Peng C. Y., Nanayakkara A., Gonzalez C., Challacombe M., Gill P. M. W., Johnson B. G., Chen W., Wong M. W., Andres J. L., Head-Gordon M., Replogle E. S., and Pople J. A. (1998) Gaussian 98 (Revision A. 7). Gaussian, Inc

Halliday A. N., Lee D.-C., Christensen J. N., Walder A. J., Freedman P. A., Jones C. E., Hall C. M., Yi W., and Teagle D. (1995) Recent developments in inductively coupled plasma magnetic sector multiple collector mass spectrometry. *International J. of Mass Spectrometry and Ion Processes* **146,** 21–33.

Hariharan P. C. and Pople J. A. (1973) Influence of polarization functions on molecular-orbital hydrogenation energies. *Theoretica Chimica Acta* **28,** 213–222.

Hariharan P. C. and Pople J. A. (1974) Accuracy of Ah equilibrium geometries by single determinant molecular-orbital theory. *Molecular Physics* **27,** 209–214.

Hehre W. J., Ditchfield R., and Pople J. A. (1972) Self-consistent molecular orbital methods. XII. Further extensions of Gaussian-type basis sets for use in molecular orbital studies *J. Chem. Phys.* **56,** 2257–2261.

Hohenberg P. and Kohn W. (1964) Inhomogeneous electron gas. *Physical Review* **136,** B864–B871.

Jarzecki A. A., Kozlowski P. M., Pulay P., Ye B. H., and Li X. Y. (1997) Scaled quantum mechanical and experimental vibrational spectra of magnesium and zinc porphyrins. *Spectrochimica Acta Part a-Molecular and Biomolecular Spectroscopy* **53,** 1195–1209.

Jarzecki A. A., Anbar A. D., and Spiro T. G. (2004) DFT analysis of $Fe(H_2O)_6^{3+}$ and $Fe(H_2O)_6^{2+}$ structure and vibrations: implications for isotope fractionation. *J. of Physical Chemistry A* **108,** 2726–2732.

Jenkins T. E. and Lewis J. (1981) A Raman investigation of some metal-(II) hexafluorosilicate-(IV) and hexafluorotitanate-(IV) salts. *Spectrochimica Acta Part a-Molecular and Biomolecular Spectroscopy* **37,** 47–50.

Johnson C. M., Skulan J. L., Beard B. L., Sun H., Nealson K. H., and Braterman P. S. (2002) Isotopic fractionation between Fe(III) and Fe(II) in aqueous solutions. *Earth and Planetary Science Letters* **195,** 141–153.

Johnson C. M., Beard B. L., Beukes N. J., Klein C., and O'Leary J. M. (2003a) Ancient geochemical cycling in the Earth as inferred from Fe isotope studies of banded iron formations from the Transvaal Craton. *Contributions to Mineral. and Petrology* **144,** 523–547.

Johnson C. M., Beard B. L., Braterman P. S., and Welch S. A. (2003b) Reply to comment on "Isotopic fractionation between Fe(III) and Fe(II) in aqueous solutions" by Thomas D. Bullen, Arthur F. White, and Cyril W. Childs *Earth and Planetary Science Letters* **206,** 233–236.

Kanno H. (1988) Hydrations of metal ions in aqueous electrolyte solutions: a Raman study. *J. Phys. Chem.* **92,** 4232–4236.

Kozlowski P. M., Jarzecki A. A., and Pulay P. (1996a) Vibrational assignment and definite harmonic force field for porphine. 1. Scaled quantum mechanical results and comparison with empirical force field *J. of Physical Chemistry* **100,** 7007–7013.

Kozlowski P. M., Jarzecki A. A., Pulay P., Li X. Y., and Zgierski M. Z. (1996b) Vibrational assignment and definite harmonic force field for porphine. 2. Comparison with nonresonance Raman data *J. of Physical Chemistry* **100,** 13985–13992.

Kozlowski P. M., Rush T. S., Jarzecki A. A., Zgierski M. Z., Chase B., Piffat C., Ye B. H., Li X. Y., Pulay P., and Spiro T. G. (1999) DFT-SQM force field for nickel porphine: Intrinsic ruffling *J. of Physical Chemistry A* **103,** 1357–1366.

Laird B. V., Ziegler T., and Roos R. (1996) *Chemical Applications of Density Functional Theory.* American Chemical Society.

Lee C. T., Yang W. T., and Parr R. G. (1988) Development of the Colle-Salvetti correlation-energy formula into a functional of the electron-density. *Physical Review B* **37,** 785–789.

Marechal C. N., Telouk P., and Albarede F. (1999) Precise analysis of copper and zinc isotopic composition by plasma-source mass spectrometry. *Chem. Geol.* **156,** 251–273.

Matthews A., Zhu X.-K., and O'Nions K. (2001) Kinetic iron stable isotope fractionation between iron (II) and (III) complexes in solution. *Earth and Planetary Science Letters* **192,** 81–92.

McManus J., Nägler T., Siebert C., Wheat C. G., and Hammond D. (2002) Oceanic molybdenum isotope fractionation: Diagenesis and hydrothermal ridge flank alteration. *Geochemistry, Geophysics, Geosystems* **3,** 1078.

Mennucci B., Cances E., and Tomasi J. (1997) Evaluation of solvent effects in isotropic and anisotropic dielectrics and in ionic solutions with a unified integral equation method: Theoretical bases, computational implementation and numerical applications. *J. of Physical Chemistry B* **101,** 10506–10517.

Mennucci B., Cammi R., and Tomasi J. (1999) Analytical free energy second derivatives with respect to nuclear coordinates: Complete formulation for electrostatic continuum solvation models. *J. Chem. Phys.* **110,** 6858–6870.

Miertus S., Scrocco E., and Tomasi J. (1981) Electrostatic interaction of a solute with a continuum-a direct utilization of ab initio molecular potentials for the prevision of solvent effects. *Chem. Physics* **55,** 117–129.

Nakagawa I. and Simanouchi T. (1964) Infrared absorption spectra of aquo complexes and the nature of co-ordination bonds. *Spectrochimica Acta* **20,** 429–439.

O'Neil J. R. (1986) Theoretical and experimental aspects of isotopic fractionation. In *Stable Isotopes in High Temperature Geological Processes* (ed. J. W. Valley et al.), Vol. **16pp.** 1–40, Mineralogical Society of America.

Polyakov V. B. (1997) Equilibrium fractionation of the iron isotopes: Estimation from Mossbauer spectroscopy data. *Geochim. Cosmochim. Acta* **61,** 4213–4217.

Polyakov V. B. and Mineev S. D. (2000) The use of Mossbauer spectroscopy in stable isotope geochemistry. *Geochim. Cosmochim. Acta* **64,** 849–865.

Rassolov V. A., Pople J. A., Ratner M. A., and Windus T. L. (1998) 6-31G* basis set for atoms K through Zn. *J. Chem. Phys.* **109,** 1223–1229.

Rehkamper M., Frank M., Hein J. R., Porcelli D., Halliday A., Ingri J., and Liebetrau V. (2002) Thallium isotope variations in seawater and hydrogenetic, diagenetic and hydrothermal ferromanganese deposits. *Earth and Planetary Science Letters* **197,** 65–81.

Richet P., Bottinga Y., and Javoy M. (1977) A review of hydrogen, carbon, nitrogen, oxygen, sulfur and chlorine stable isotope fractionation among gaseous molecules. *Annu. Rev. of Earth and Planetary Science* **5,** 65–110.

Roe J. E., Anbar A. D., and Barling J. (2003) Nonbiological fractionation of Fe isotopes: evidence of an equilibrium isotope effect. *Chem. Geol.* **195,** 69–85.

Rudolph W. W. and Pye C. C. (2000) Aqueous solution chemistry of scandium (III) studied by Raman spectroscopy and ab initio molecular orbit calculations. *J. Solution Chem.* **29,** 955–986.

Schafer A., Horn H., and Ahlrichs R. (1992) Fully optimized contracted Gaussian-basis sets for atoms Li to Kr. *J. Chem. Phys.* **97,** 2571–2577.

Schauble E. A., Rossman G. R., and Taylor H. P. (2001) Theoretical estimates of equilibrium Fe-isotope fractionations from vibrational spectroscopy. *Geochim. Cosmochim. Acta* **65,** 2487–2597.

Schauble E. A. (2004) Applying stable isotope fractionation theory to new systems. *Rev. in Mineral. and Geochemistry* **55,** 65–111.

Sharma M., Polizzotto M., and Anbar A. D. (2001) Iron isotopes in hot springs along the Juan de Fuca Ridge. *Earth and Planetary Science Letters* **194,** 39–51.

Siebert C., Nägler T. F., von Blanckenburg F., and Kramers J. D. (2003) Molybdenum isotope records as a potential new proxy for paleoceanography. *Earth and Planetary Science Letters* **211,** 159–171.

Skulan J. L., Beard B. L., and Johnson C. M. (2002) Kinetic and equilibrium Fe isotope fractionation between aqueous Fe(III) and hematite. *Geochim. Cosmochim. Acta* **66,** 2995–3015.

Urey H. C. (1947) The thermodynamic properties of isotopic substances. *J. of the Chem. Society*, 562–581.

Walczyk T. and von Blanckenburg F. (2002) Natural iron isotope variations in human blood. *Science* **295,** 2065–2066.

Welch S. A., Beard B. L., Johnson C. M., and Braterman P. S. (2003) Kinetic and equilibrium Fe isotope fractionation between aqueous Fe(II) and Fe(III). *Geochim. Cosmochim. Acta* **67,** 4231–4250.

Wilson E. B., Cross P. C., and Decius J. C. (1955) *Molecular Vibrations: The Theory of Infrared and Raman Vibrational Spectra.* pp. 182–193. Dover.

Wombacher F., Rehkamper M., Mezger K., and Munker C. (2003) Stable isotope compositions of cadmium in geological materials and meteorites determined by multiple-collector ICPMS. *Geochim. Cosmochim. Acta* **67,** 4639–4654.

Zhu X.-K., O'Nions K., Guo Y., and Reynolds B. C. (2000) Secular variation of iron isotopes in North Atlantic Deep Water. *Science* **287,** 2000–2002.